nature communications

Article

https://doi.org/10.1038/s41467-026-71344-9

Recombinant haemostatic protein for therapeutic substitution of platelet function via tripartite haemostatic mechanisms in thrombocytopenic male mice

Received: 20 July 2025

Accepted: 20 March 2026

Published online: 01 April 2026

Check for updates

Chul-Gyun Lim[1,5], Joonha Lee[1,5], Gyeongseo Suk[1], Jong-Min Kim[2], Hyunbo Shim[3], Hae Woong Choi[1], Ji-Young Park[2], Soon Jun Hong[4] & Chungho Kim[1]

Platelets play a pivotal role in haemostasis during both external trauma and spontaneous vascular injury. Thrombocytopenia, an abnormally low platelet count caused by conditions such as autoimmune disease or chemotherapy, can lead to excessive bleeding and potentially serious medical complications. Although platelet transfusion remains the most direct and conventional treatment for thrombocytopenia, its clinical use is limited by donor scarcity and safety concerns. In this study, we developed a recombinant Fc-fusion protein composed of fibrinogen-, thrombin-, and collagen-binding modules—representing a tripartite haemostatic mechanism—derived from endogenous proteins or single-chain variable fragments. Intravenous administration of this recombinant protein significantly reduced bleeding in thrombocytopenic male mice subjected to liver laceration by targeting the injury site and promoting fibrin network formation. Importantly, the protein did not induce detectable pulmonary microthrombi and suppressed spontaneous intestinal bleeding in a chemotherapy-induced thrombocytopenic male mouse model. Taken together, these findings suggest that the recombinant protein can recruit fibrinogen and thrombin to collagen-exposed wound sites, facilitating fibrin gel formation even in the absence of platelets. Thus, it may serve as a promising alternative to conventional platelet transfusion therapy in thrombocytopenic conditions.

Haemostasis is a tightly regulated process that prevents bleeding and preserves vascular integrity following blood vessel injury. Platelets play a central role in this process by recognising exposed collagen at the injury site binding to fibrinogen to recruit additional platelets and form platelet aggregates, and initiating fibrin gel formation through activation of the coagulation proteolytic cascade[1]. Given the critical role of platelets in haemostasis a reduced platelets count, or thrombocytopenia, poses a serious risk of bleeding during external injury or surgical intervention. Even in the absence of overt trauma thrombocytopenic conditions often fail to prevent spontaneous bleeding[2],

[1]Department of Life Sciences, Korea University, Seoul, Republic of Korea. [2]Department of Clinical Pharmacology and Toxicology, Korea University Anam Hospital, Korea University College of Medicine, Seoul, Republic of Korea. [3]Department of Life Science, Ewha Womans University, Seoul, Republic of Korea. [4]Department of Cardiology, Cardiovascular Center, Korea University Anam Hospital, Korea University College of Medicine, Seoul, Republic of Korea. [5]These authors contributed equally: Chul-Gyun Lim, Joonha Lee. e-mail: chungho@korea.ac.kr

which may manifest in the skin or mucous membranes and, more seriously, as an increased risk of intracranial haemorrhage[3,4].

Immune thrombocytopenia is a representative example of such a condition which results from the production of platelet-specific autoantibodies, leading to Fc-mediated phagocytic clearance of autoantibody-bound platelets in the spleen[5]. Various treatments have been developed for this disease. One strategy involves immunosuppressive therapy using corticosteroids[6,7] or rituximab[8]. Another approach aims to inhibit platelet destruction in the spleen either through intravenous immunoglobulin, which competes with platelets for Fc receptor binding and inhibits phagocytosis[9], or via surgical removal of the spleen[10]. Thrombopoietin receptor agonists have also been introduced to stimulate platelet production[11].

Chemotherapy in patients with cancer represents another major cause of thrombocytopenia primarily due to the proliferation-inhibitory effects of chemotherapeutic agents on bone marrow stem cells or megakaryocytes[12,13]. In cancer patients with thrombocytopenia typical management strategies include dose reduction during chemotherapy or switching to alternative agents, though both may compromise tumour remission rates[14]. Thrombopoietin-receptor agonists have also been used in this context[15].

Although multiple treatment options exist platelet transfusion remains the most effective strategy for managing thrombocytopenia[16]. However despite its clinical importance—particularly for thrombocytopenic patients undergoing cancer therapy or surgery—platelet transfusion is significantly limited by short shelf life, donor dependency, and the risk of alloimmunization. Therefore a functionally active, intravenously injectable and manufacturable haemostatic agent that can operate independently of endogenous platelets would represent a compelling therapeutic advancement. Nevertheless restoring haemostasis under thrombocytopenic conditions remains highly challenging. Unlike bleeding disorders caused by mutations or deficiencies in specific coagulation factors which can often be managed by factor supplementation[17], such haemostatic agent must replicate the multiple and complex functions of natural platelets. In addition although several haemostatic agents have demonstrated impressive efficacy in accelerating clot formation in the presence of platelets[18], truly functional agents must maintain haemostatic activity even when platelet counts are severely reduced. More importantly they must not induce unwanted thrombus formation, which could result in life-threatening complications. Recently several groups have developed platelet substitutes using engineered biomaterials, for examples, ultrasoft microgel-based platelet-like particles that interact with fibrin networks[19] and plasmin-responsive liposomal nanoparticles that expose phosphatidylserine to promote coagulation at injury sites[20].

In this study we adopted a different approach and present a recombinant protein-based haemostatic agent engineered by fusing human-derived endogenous protein domains or single-chain variable fragments (scFv) capable of binding to fibrinogen, thrombin or collagen—three key components involved in haemostatic plug formation—to the Fc fragment of immunoglobulin G. We demonstrate that these recombinant proteins when administered intravenously in a thrombocytopenic mouse model, were effectively recruited to injury sites, enhanced fibrinogen deposition, and significantly reduced bleeding without inducing pathological thrombus formation. In vitro mechanistic studies suggest that their haemostatic activity is attributable to fibrinogen binding and crosslinking as well as their ability to increase the local concentration of thrombin at collagen-exposed wound sites. Furthermore administration of these recombinant proteins significantly reduced spontaneous intestinal bleeding. Collectively these findings indicate that our recombinant haemostatic proteins, through their combined functional properties, can support haemostasis under thrombocytopenic conditions, and may offer a potential transfusion-independent platform for managing thrombocytopenia.

Results

Design of an endogenous protein domain-based haemostatic protein

During haemostasis platelets facilitate fibrin gel formation at injury sites by recognising exposed collagen, recruiting fibrinogen and initiating thrombin-mediated fibrin polymerisation (Fig. 1a, upper panel). We hypothesised that a recombinant protein with binding affinities for collagen and prothrombin could locally concentrate prothrombin at the lesion which would then be activated into α-thrombin by factor Xa through the extrinsic coagulation pathway[21]. In addition if the protein were equipped with fibrinogen-binding activity, the localised thrombin could convert the recruited fibrinogen into fibrin, exposing additional fibrin-binding sites and enabling further recruitment of fibrinogen. This would promote fibrin network formation at the injury site thereby acting in a platelet-like manner (Fig. 1a, lower panel).

To test this hypothesis we first evaluated whether localising such activities could generate a fibrin gel with sufficient mechanical resistance to reduce leakage under defined pressure in the absence of other platelet-derived functions, such as their physical mass or contractile activity[22,23]. To this end we applied 200 µL of fibrinogen solution at its physiological concentration (5 mg/mL) through filters coated with varying concentrations of α-thrombin (Fig. 1b), or conversely, passed α-thrombin solutions at various concentrations through fibrinogen-coated filters (Fig. 1c). Centrifugation at 650 × *g* was used to simulate a blood pressure of ~133 mmHg for 5 min. In both scenarios leakage through the filter gradually decreased in a thrombin concentration-dependent manner, suggesting that sufficient fibrin network formation may limit fluid passage.

Next we generated a recombinant protein with binding affinities for collagen, prothrombin and fibrinogen by assembling three endogenous protein domains with these functions. For fibrinogen binding we used the N-terminal region of the fibrinogen α-chain, here referred to as FA. This region includes the signal peptide fibrinopeptide A, and the Gly-Pro-Arg (GPR) motif, which is exposed upon thrombin cleavage and mediates binding to other fibrinogen molecules[24]. It also contains residues that interact with thrombin exosite I a substrate docking site that facilitates efficient cleavage[25]. Because FA cannot bind fibrinogen until it is cleaved by thrombin activated at the injury site we anticipated that this region could act as a 'safety lock', minimising potential non-specific fibrinogen aggregation.

To enable thrombin interaction we incorporated the Apple 1 domain of coagulation factor XI, known to mediate direct binding to prothrombin[26]. This domain was designated as PT. Finally to confer targeting specificity for damaged vessels, we included the collagen-binding A1 domain of von Willebrand factor[27]. These three functional domains were fused to the Fc fragment to enhance avidity and simplify purification resulting in the recombinant construct FA-PT-A1 (Fig. 1d and Supplementary Fig. 1a), whose structure was predicted using AlphaFold2[28]. The recombinant FA-PT-A1 protein was expressed in 293-F cells and purified by protein A affinity chromatography followed by pH elution (Fig. 1e). Sodium dodecyl sulphate-polyacrylamide gel electrophoresis (SDS-PAGE) analysis confirmed Fc-mediated dimerisation of FA-PT-A1 (Fig. 1f). Enzyme-linked immunosorbent assay (ELISA) confirmed binding of FA-PT-A1 to prothrombin and collagen (Fig. 1g, h). As expected binding to fibrinogen in the absence of thrombin was minimal, but became evident upon thrombin activation (Fig. 1i). Subsequent surface plasmon resonance (SPR) analysis showed binding affinity (K_D) 674.3 nM for prothrombin, 8.48 µM for collagen, 160 nM for fibrinogen (Supplementary Fig. 1b).

Design and construction of a scFv-based haemostatic protein

To further test our hypothesis we developed an alternative recombinant protein using scFv with binding affinity for collagen, fibrinogen and thrombin. Using a previously constructed phage display scFv library[29] we isolated clones binding to collagen after three rounds of

https://doi.org/10.1038/s41467-026-71344-9

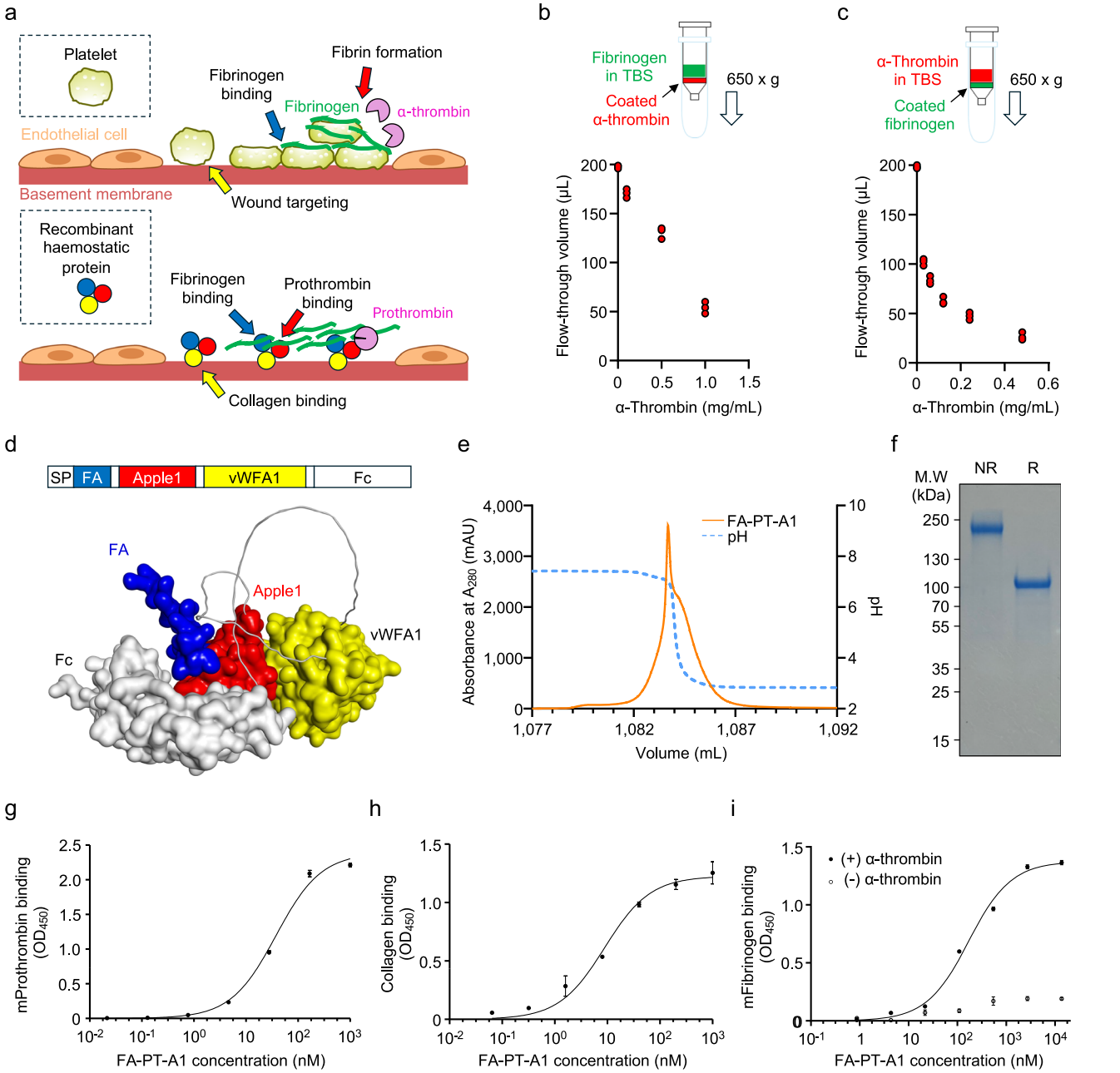

Fig. 1 | Recombinant protein FA-PT-A1 with binding affinities for fibrinogen, prothrombin and collagen. a Schematic diagram illustrating the hypothesised essential functions of platelets and recombinant haemostatic proteins during haemostasis. **b** A 5 mg/mL fibrinogen solution was applied to spin columns pre-coated with different concentrations of α-thrombin. Flowthrough volumes were measured as a proxy for fibrin network permeability and shown as dot plots ($n = 3$). **c** Varying concentrations of α-thrombin were applied to spin column inserts pre-coated with fibrinogen and analysed as in (**b**). **d** Domain structure of FA-PT-A1 and its AlphaFold-predicted 3D structure. SP signal peptide, vWF von Willebrand factor. **e** Fc affinity chromatography elution profile of FA-PT-A1. **f** SDS-PAGE analysis of FA-PT-A1 under non-reducing (NR) and reducing (R) conditions. Representative data for at least 3 independent experiments are shown. Source data are provided as a Source data file. Binding of FA-PT-A1 at varying concentrations to mouse prothrombin (**g**), bovine collagen (**h**), and mouse fibrinogen in the presence or absence of α-thrombin (**i**) was analysed by ELISA. Black lines indicate non-linear fitting using a one-site specific binding model. Experiments were repeated independently at least 3 times with similar results. Error bars represent the mean ± SE ($n = 3$, technical replicates).

panning (Fig. 2a, b), as well as clones binding to fibrinogen (Fig. 2c, d) and prothrombin (Fig. 2e, f). In all screenings the output-to-input ratio —an indicator of target-specific phage binding[30]—increased (Fig. 2a, c, e), indicating successful enrichment.

Sequencing of positive clones identified eight unique collagen binders 10 fibrinogen binders and 18 prothrombin binders (Fig. 2b, d, f; clone names indicated in bold). Three scFv clones—T17 (thrombin-binding), C6 (collagen-binding) and F7 (fibrinogen-binding)—were selected based on clone abundance, binding affinity, compatibility with fibrin gel formation and expression level (Supplementary Fig. 2). These scFvs were linked via Gly-Ser flexible linkers[31] to allow each module to function independently so that their activities are not dependent on domain order, and the construct was fused with a signal peptide and twin-Strep (TST) tag[32] at the N-terminus and an Fc domain at the C-terminus, resulting in the construct T17-C6-F7 (Fig. 2g and Supplementary Fig. 3a). The purified protein T17-C6-F7 (Fig. 2g, h),

https://doi.org/10.1038/s41467-026-71344-9

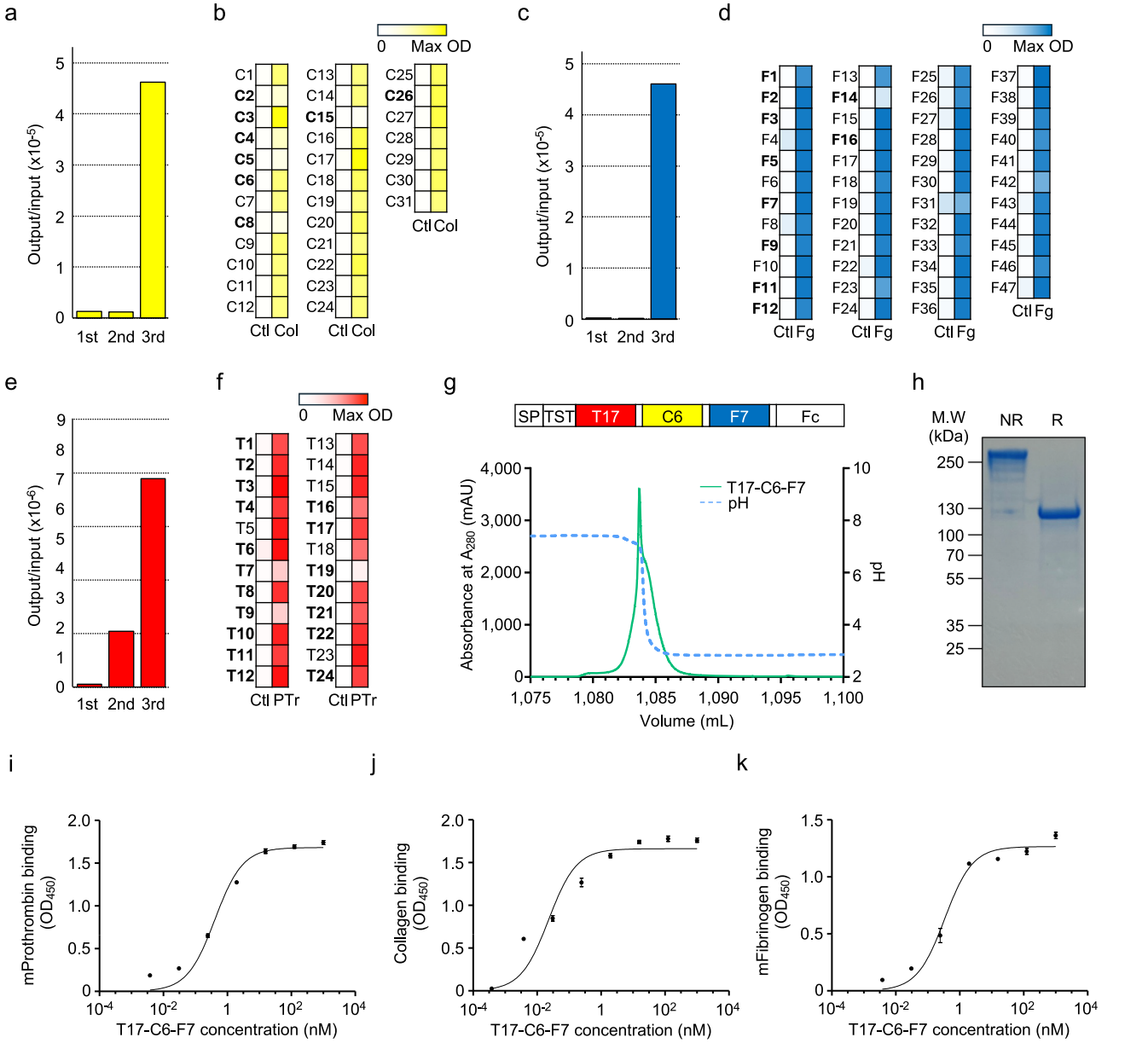

Fig. 2 | Recombinant protein T17-C6-F7 consisting of scFvs targeting prothrombin, collagen and fibrinogen. a Output-to-input ratios of phage titres from three rounds of scFv phage library panning on bovine collagen. **b** Clones obtained from the third round of panning against collagen were tested for their binding to control protein (Ctl; glutathione S-transferase) or collagen by ELISA. Optical absorbance at 280 nm was measured using a spectrophotometer and represented as a colour gradient. Clones in bold indicate unique amino acid sequences. Output-to-input ratios and ELISA results of fibrinogen-binding clones (**c**, **d**) and prothrombin-binding clones (**e**, **f**), respectively, presented similarly to (**a**, **b**). **g** Schematic diagram of the T17-C6-F7 construct (top) and chromatogram of its purification elution profile (bottom). TST, twin-Strep tag. **h** SDS-PAGE analysis of purified T17-C6-F7 under NR and R conditions. Representative data for at least 3 independent experiments are shown. Source data are provided as a Source data file. Binding of T17-C6-F7 to mouse prothrombin (**i**), bovine collagen (**j**) and mouse fibrinogen (**k**), analysed as in Fig. 1. Experiments were repeated independently at least 3 times with similar results. Error bars represent the mean ± SE ($n = 3$, technical replicates).

exhibited binding to prothrombin, collagen and fibrinogen, as measured by ELISA (Fig. 2i–k). SPR analysis further determined the binding affinity to be 490.7 nM for prothrombin 210.3 nM for collagen and 2.57 µM for fibrinogen, respectively (Supplementary Fig. 3b).

Haemostatic effects of FA-PT-A1 and T17-C6-F7 in thrombocytopenic mice

To evaluate haemostatic efficacy we first determined the plasma half-lives of FA-PT-A1 and T17-C6-F7 in mice using sandwich ELISA. To minimise background signals from anti-Fc detection in serum we inserted a 2B8 tag[33] immediately after the signal peptide, allowing specific capture via an anti-2B8-coated surface. ELISA on blood samples (50 µL) collected from the left jugular vein at 1, 6, 12, 26.5, 36, 51 and 73 h post-injection of the recombinant proteins (5 mg/kg) revealed plasma half-lives of 41.47 ± 2.12 h for FA-PT-A1 and 27.79 ± 1.16 h for T17-C6-F7 (Fig. 3a), suggesting a practical time window of ~24 h for efficacy evaluation. At 48 h after injection the recombinant proteins were detected predominantly in the liver (Supplementary Fig. 4), consistent with clearance pathways commonly observed for biologics[34]. In vitro ELISA suggested that the recombinant proteins minimally bind to plasma proteins such as albumin (Supplementary Fig. 5a) and can retain their intended interaction with fibrinogen in a

https://doi.org/10.1038/s41467-026-71344-9

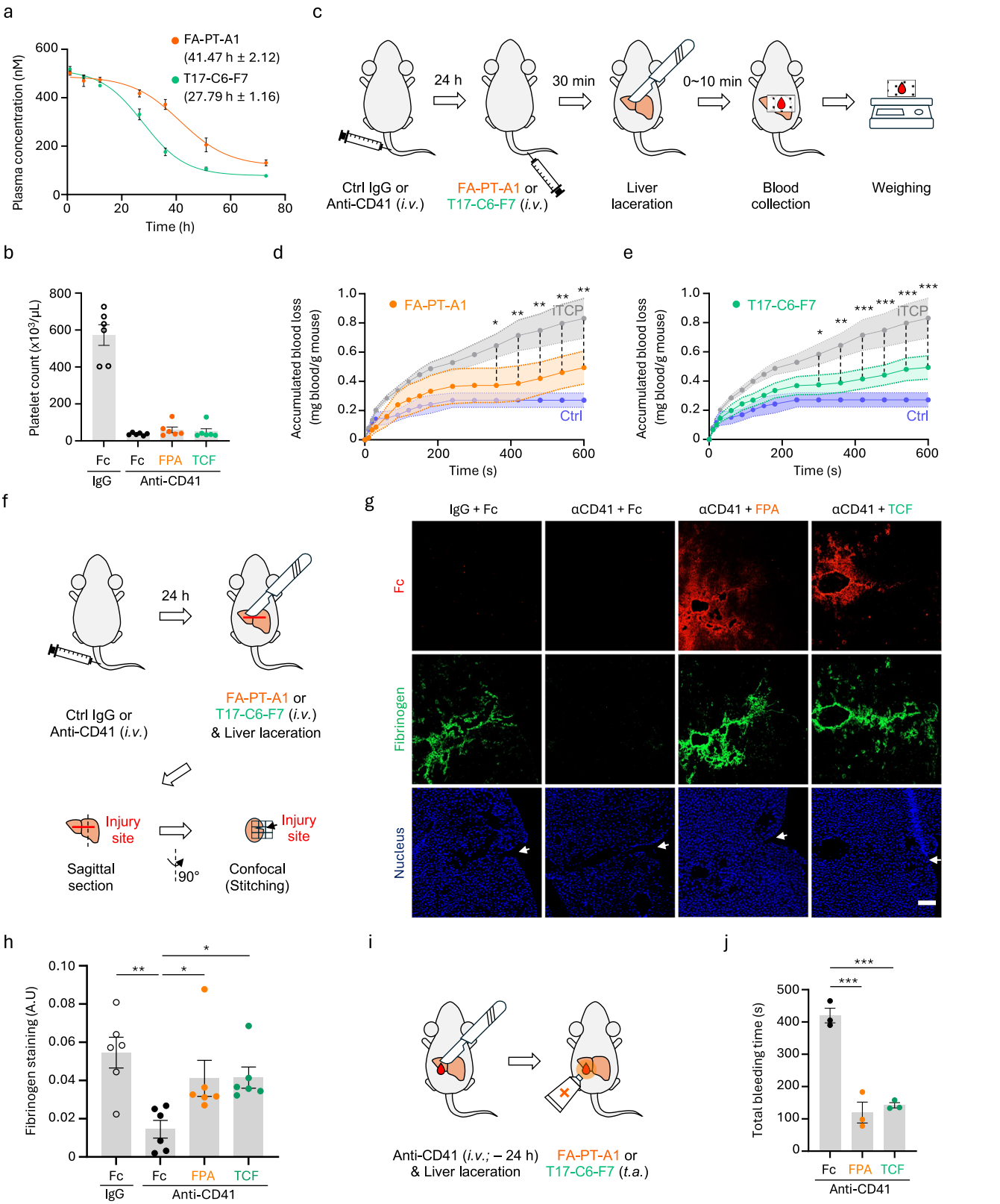

plasma environment (Supplementary Fig. 5b, c). Because the recombinant proteins were designed to function independently of platelets and contain no motifs that directly bind them their presence did not have significant effects on platelet aggregation (Supplementary Fig. 5d) or platelet adhesion (Supplementary Fig. 5e) in vitro.

Next to assess the haemostatic efficacy of the recombinant proteins, thrombocytopenia was induced using an anti-CD41 antibody[35]. Platelet counts decreased to 30–60 × 10^3/μL which is less than 10% of the normal level (~573 × 10^3/μL), by day 1 post-injection of anti-CD41 antibodies (Fig. 3b), indicating severe thrombocytopenia[36]. As expected the reduced platelet count was accompanied by decreases in ATP, ADP and thromboxane A_2 levels, factors derived from platelets, while plasma thrombin level was not changed significantly (Supplementary Fig. 5f–i). Administration of FA-PT-A1 or T17-C6-F7 did not significantly

Fig. 3 | Haemostatic effect of FA-PT-A1 and T17-C6-F7 in thrombocytopenic mice. a Plasma concentrations of 2B8-tagged FA-PT-A1 and T17-C6-F7 measured by ELISA at the indicated time points and plotted as dots. Error bars represent the mean ± SE ($n = 3$ mice per group). **b** Platelet counts for each condition. Error bars represent the mean ± SE ($n = 6$ mice per group). IgG control for anti-CD41 antibody; Fc, Fc control for recombinant haemostatic protein; FPA, FA-PT-A1; TCF, T17-C6-F7. **c** Schematic diagram of the experimental timeline. i.v., intravenous injection. **d** Time-dependent accumulated blood loss following liver laceration in the Fc control (Ctrl; blue), anti-CD41-injected (iTCP; grey), and anti-CD41 plus FA-PT-A1-injected mice (orange). Each graph represents the mean ± SE ($n = 6$ mice per group). Statistical analysis was performed using two-way ANOVA with Dunnett's test. *, $p \le 0.05$ (360 s: 0.0173); **, $p \le 0.01$ (420 s: 0.0033; 480 s: 0.0033; 540 s: 0.0026; 600 s: 0.0025); ***, $p \le 0.001$. iTCP, induced-thrombocytopenia. Source data are provided as a Source data file. **e** Time-dependent accumulated blood loss of T17-C6-F7-treated thrombocytopenic mice (green), as in (**d**). Statistical analysis was performed using two-way ANOVA with Dunnett's test. *, $p \le 0.05$ (300 s: 0.0213); **, $p \le 0.01$ (360 s: 0.0036); ***, $p \le 0.001$ (420 s: 0.0006; 480 s: 0.0004; 540 s: 0.0003; 600 s: 0.0001). iTCP, induced-thrombocytopenia. Source data are provided as a Source data file. **f** Schematic diagram of the confocal imaging (LSM 900, Zeiss) of liver cryosections. **g** Representative stitched confocal images of liver sections stained with anti-Fc antibody (red) to detect Fc control, FA-PT-A1 (FPA), and T17-C6-F7 (TCF), and with anti-fibrinogen α-chain antibody (green) are shown. Nuclei are counterstained with DAPI. White arrows indicate the laceration site. Scale bar, 100 μm. **h** Fibrinogen fluorescence intensities normalised to tissue area and shown as a bar graph, with individual values indicated as dots. Error bars represent the mean ± SE ($n = 6$ sections from six mice for each condition). One-way ANOVA with Dunnett's test: *, $p \le 0.05$ (anti-CD41/Fc vs. anti-CD41/FPA: 0.0419; anti-CD41/Fc vs. anti-CD41/TCF: 0.0388); **, $p \le 0.01$ (IgG/Fc vs. anti-CD41/Fc: 0.0022). Source data are provided as a Source data file. **i** Schematic diagram of topical application (t.a.) of FA-PT-A1 or T17-C6-F7 (500 nM in 1% sodium alginate gel) to the lacerated liver. **j** Total bleeding time in FA-PT-A1 or T17-C6-F7-treated thrombocytopenic mice. Error bars represent the mean ± SE ($n = 3$ mice per group). One-way ANOVA with Dunnett's test: ***, $p \le 0.001$ (Fc vs FPA: 0.0002; Fc vs TCF: 0.0003). Source data are provided as a Source data file.

alter these parameters under non-injured condition (Supplementary Fig. 5f–i). For the bleeding assay thrombocytopenic mice generated by anti-CD41 injection were then subjected to a liver laceration model[37] to quantitatively measure blood loss (Fig. 3c). For comparison with the recombinant proteins an Fc-only protein was used as the appropriate control, because FA-PT-A1 and T17-C6-F7 are Fc-fusion constructs. As expected Fc control-injected thrombocytopenic mice exhibited significantly increased bleeding compared to healthy controls (Fig. 3d, e, grey vs. blue lines). In contrast mice pretreated with FA-PT-A1 or T17-C6-F7 (5 mg/kg) at 30 min before liver laceration showed a 59.5% and 59.4% reduction in blood loss, respectively, based on total blood loss measured at 600 s (Fig. 3d, e), indicating their efficacy as platelet substitutes under thrombocytopenic conditions. Histological staining of liver sections using anti-Fc antibodies (Fig. 3f) confirmed wound-specific accumulation of both proteins compared to the Fc control-injected groups (Fig. 3g, top and bottom panels), while platelet staining was observed only at the wound site in the Fc control-injected groups (Supplementary Fig. 6). Fibrinogen staining which was minimal in Fc-treated thrombocytopenic mice, was restored in mice treated with the recombinant proteins and resembled that of healthy controls (Fig. 3g, middle panels). Quantification confirmed significant increases in fibrinogen staining near the wound in mice injected with recombinant proteins (Fig. 3h). Furthermore topical application of the recombinant proteins in 1% (w/v) sodium alginate hydrogel (Fig. 3i) also reduced bleeding from lacerated livers in thrombocytopenic mice (Fig. 3j, Supplementary Movies 1, 2 and Supplementary Fig. 7), further supporting their haemostatic potential. Nonetheless the absence of other platelet functions may not allow complete and sustained haemostasis. Indeed even after the recombinant proteins induced initial haemostasis at the injured tail, rebleeding was observed in thrombocytopenic mice (Supplementary Fig. 8). Taken together these data suggest that the recombinant proteins mitigate bleeding under thrombocytopenic conditions by targeting wounds and possibly promoting fibrin network formation, although they do not fully substitute for the diverse functional roles of platelets.

Safety evaluation of the recombinant haemostatic proteins

To evaluate potential side effects we administered the recombinant haemostatic proteins to mice three times at 4-day intervals and assessed their safety profiles (Fig. 4a). Throughout the dosing period no significant changes in body weight were observed across the groups (Supplementary Fig. 9a). Core body temperature also remained stable and comparable among all groups (Supplementary Fig. 9b). Plasma obtained on day 11 showed non-detectable levels of antigen-specific total IgE in all groups (Supplementary Fig. 9c) indicating the absence of IgE-mediated hypersensitivity. The stable body-temperature profiles were consistent with this absence of allergic responses. Peripheral blood collected on days 2 and 11 was also analysed for immune-cell composition. Flow cytometry revealed no significant or minimal alterations in $CD3^+$ T cells $CD19^+$ B cells, $CD45^+$ leucocytes, or $Ly6C^+$ inflammatory cells in FA-PT-A1 or T17-C6-F7-treated mice relative to controls (Fig. 4b, c and Supplementary Fig. 9d, e). These results indicate that repeated administration of the recombinant proteins does not induce meaningful changes in the major immune-cell populations in peripheral blood. Furthermore to evaluate potential organ-level toxicity, kidneys from all treatment groups were collected for H&E-based histopathological examination (Supplementary Fig. 9f). Independent pathological assessment demonstrated well-preserved glomerular architecture without evidence of mesangial expansion tuft retraction, or capillary loop distortion. Likewise the renal tubules and collecting ducts exhibited normal epithelial morphology with no signs of cellular degeneration, luminal obstruction, or inflammatory infiltrates. Overall no histopathological abnormalities attributable to repeated dosing of the recombinant proteins were identified.

To evaluate potential prothrombotic side effects lung tissues from mice after repeated dosing were analysed histologically (Fig. 4a). Pulmonary microthrombi frequently occur in pathological conditions due to the lung's dense capillary network which readily traps circulating thrombi[38]. A 10-min mucin injection served as a prothrombotic control[39]. Anti-CD41/DAPI staining revealed that clustered staining patterns—defined as particles larger than 30 μm^2 approximately the area of a single spread platelet and used here as indicative of microthrombi[40]—were prevalent in mucin-injected mice, whereas such patterns were barely detected in the recombinant protein-injected groups and in Fc control-injected groups (Fig. 4d). To quantify platelet staining we converted the microscopy images into a binary format and performed particle analysis to measure the stained areas (Supplementary Fig. 10). Mucin-injected mice showed a substantial increase in both the total area occupied by such particles (Fig. 4e) and the number of microthrombi (Fig. 4f) per microscopic field. In contrast neither FA-PT-A1 nor T17-C6-F7 induced such features indicative of pulmonary microthrombus formation. These results suggest that intravenous injection of recombinant proteins may not trigger a prothrombotic response.

Functional and mechanistic properties of human FA-PT-A1

The demonstrated haemostatic efficacy (Fig. 3) and safety profile (Fig. 4) of FA-PT-A1 support its potential as a platelet substitute for therapeutic development. To reduce the risk of immunogenicity, all mouse-derived domains in FA-PT-A1 were replaced with their human counterparts (Fig. 5a and Supplementary Fig. 11a). The resulting human

https://doi.org/10.1038/s41467-026-71344-9

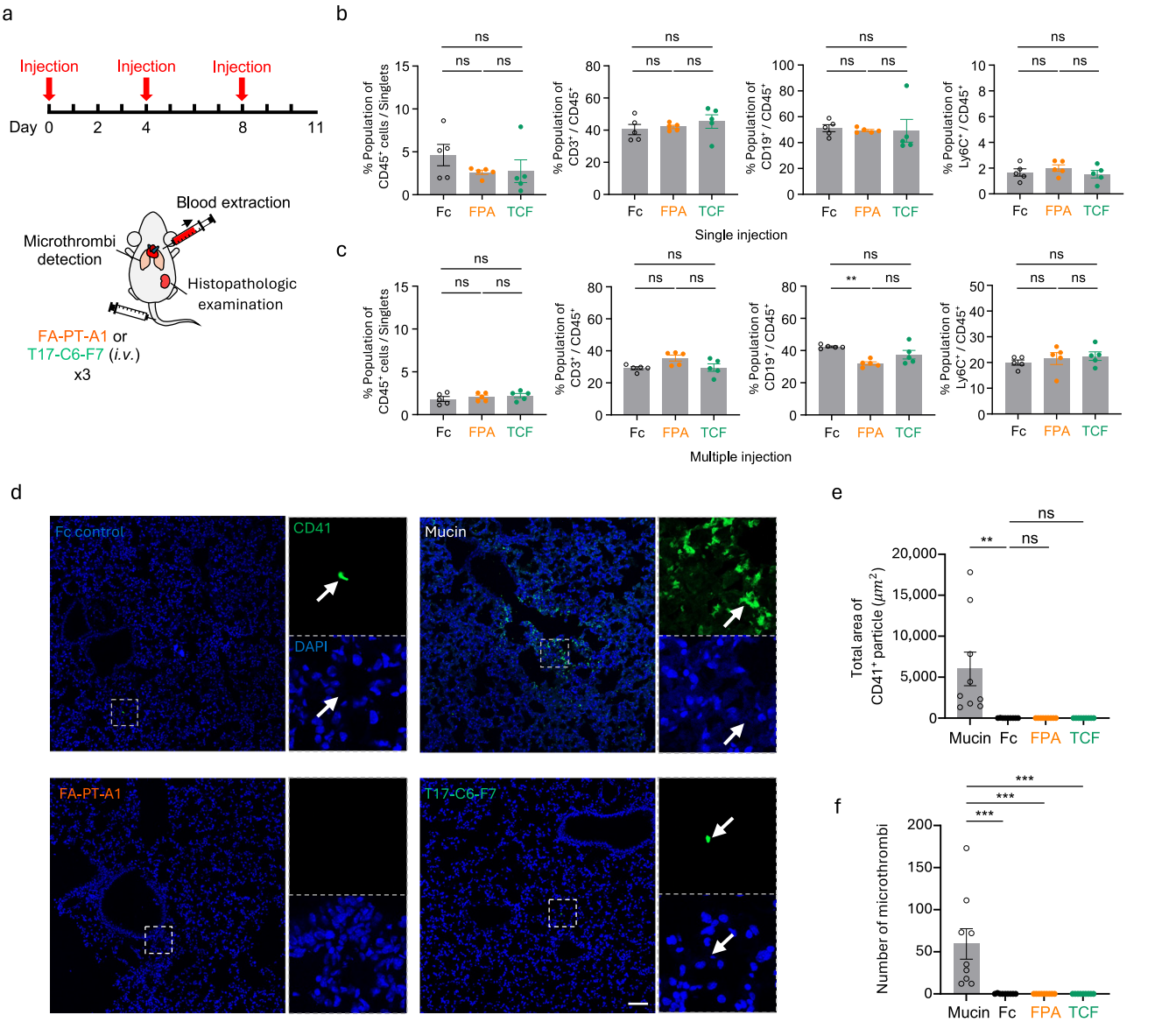

Fig. 4 | Safety evaluation of the recombinant haemostatic proteins. a Schematic diagram of the experimental model: mice were injected with FA-PT-A1, T17-C6-F7 (5 mg/kg), Fc control (5 mg/kg) for 3 multiple injections for 4 d term and euthanised on day 11. Mucin (0.5 mg/kg) was injected 10 min before euthanasia on day 11. Lungs were cryosectioned and imaged using confocal microscopy. Nine adjacent fields were stitched into one image. The kidney was harvested and fixed in 4% paraformaldehyde, paraffin sectioned for H&E staining. Whole blood was collected via cardiac puncture for immune cell flow cytometry ($n = 5$ mice per group). **b** Peripheral blood collected on days 2 and 11 was analysed for immune-cell composition. Flow cytometry against the population of $CD3^+$ T cells $CD19^+$ B cells, $CD45^+$ leucocytes, or $Ly6C^+$ inflammatory cells in FA-PT-A1 or T17-C6-F7-treated mice were analysed on day 2 (single injection) **c** day 11 (multiple injections). Error bars represent the mean ± SE ($n = 5$ mice per group). One-way ANOVA with Tukey's test: **, $p \le 0.01$ (Fc vs FPA: 0.0025); ns, not significant. Source data are provided as a Source data file. **d** Representative immunofluorescence images of lung tissue stained with anti-CD41 antibody (green) and nuclei counterstained with DAPI (blue). Scale bar, 100 μm. Digitally magnified regions are outlined with dotted lines. Arrows indicate $CD41^+$ particles. **e** Total area of $CD41^+$ particles is shown as a scatter plot. Error bars represent the mean ± SE ($n = 9$ sections from five mice per group). One-way ANOVA with Tukey's test: **, $p \le 0.01$ (mucin vs. Fc: 0.0012; mucin vs. FPA: 0.0012; mucin vs. TCF: 0.0012); ns, not significant. Source data are provided as a Source data file. **f** Number of microthrombi, defined as $CD41^+$ particles exceeding 30 μm^2, are shown as a scatter plot ($n = 9$ sections from five mice per group). Error bars represent the mean ± SE. One-way ANOVA with Tukey's test: ***, $p \le 0.001$ (mucin vs. Fc: 0.0003; mucin vs. FPA: 0.0003; mucin vs. TCF: 0.0003). Source data are provided as a Source data file.

recombinant protein hFA-PT-A1, was expressed in 293-F cells and purified using protein A affinity column (Fig. 5b, c). ELISA confirmed its binding affinities to human prothrombin collagen and human fibrinogen (Fig. 5d–f). As with the mouse version, binding to human fibrinogen was dependent on thrombin-mediated activation (Fig. 1i). Because commercial human collagen was unavailable bovine collagen was used under the assumption that the conserved Gly-X-Y motif and triple-helical structure are more critical than species-specific sequences[41]. SPR analysis of these interacting pairs determined binding affinity of 1.56 μM for prothrombin 238.6 nM for collagen and 54.8 nM for fibrinogen, respectively (Supplementary Fig. 11b).

To mimic the haemostatic process in vitro hFA-PT-A1 was applied to a collagen-coated surface and incubated with thrombin, followed by assessment of surface thrombin activity using the thrombin-specific fluorogenic substrate Z-GGR-AMC (Fig. 5g, inset). As expected deletion of either the prothrombin-binding PT domain or the collagen-binding A1 domain significantly reduced thrombin activity on the collagen surface, whereas deletion of the fibrinogen-binding FA domain had

minimal effect, highlighting the importance of PT and A1 in thrombin localisation. We also evaluated fibrin network formation by measuring turbidity at 350 nm. Addition of hFA-PT-A1 to a fibrinogen solution at a 1:10 molar ratio accelerated fibrin polymerisation as indicated by a shortened time to maximal turbidity and an increased final turbidity value (Fig. 5h), suggesting enhanced fibrin network density and maturation. Confocal microscopy further revealed that hFA-PT-A1 promoted denser fibrin gel structures compared to control (Fig. 5i, j). Notably deletion of the FA domain, hPT-A1(ΔFA), markedly reduced this effect, whereas deletion of either the PT or A1 domain, hFA-A1(ΔPT) or hFA-PT (ΔA1), had effects nearly equivalent to that of hFA-PT-A1 (Fig. 5i, j). This enhancement is likely due to the Fc-mediated dimeric nature of hFA-PT-A1 which provides two GPR motifs (knob A) capable of binding to the hole a region in the fibrinogen γ chain[42].

Typically knob A–hole a interactions occur between two fibrin molecules simultaneously, yielding a functionality (f) of 2 based on the Flory–Stockmeyer gelation theory[43], which leads to linear protofibril formation[44] (Supplementary Fig. 12a). Occasionally trimolecular junctions also form, contributing branch points to the fibrin network[45] (Supplementary Fig. 12a). In contrast hFA-PT-A1 forms an Fc-mediated dimer that presents two knob A motifs but no hole a. Thus when two hFA-PT-A1 dimers bind independently to the two native hole a sites at each end of a protofibril, only one knob A motif from each dimer is engaged, leaving two unused knob A motifs at each end. As a result a total of four knob A motifs remain exposed, effectively increasing the protofibril functionality to $f = 4$ (Supplementary Fig. 12b). Computational simulations based on the Flory–Stockmeyer theory and the Carr–Hermans turbidity model[46] predict that this increased functionality promotes enhanced branching (Supplementary Fig. 12c) and results in denser fibrin gels (Supplementary Fig. 12d) which aligns with our experimental observations of increased fibrin gel turbidity (Fig. 5h).

Protective role of hFA-PT-A1 against intestinal haemorrhage

We further evaluated the haemostatic efficacy of hFA-PT-A1 in a mouse model. Given that hFA-PT-A1 was generated using human protein domains cross-species binding to mouse prothrombin and fibrinogen was confirmed via ELISA (Fig. 6a, b). Binding to collagen was not re-evaluated due to the expected interspecies similarity as previously noted. The plasma half-life in mice was measured as the mouse version of FA-PT-A1 (Fig. 3a), and found to be approximately 41 h (Fig. 6c).

The haemostatic efficacy of hFA-PT-A1 was next evaluated using the same liver-laceration model described in Fig. 3c where it exhibited a comparable reduction in blood loss (Fig. 6d). Notably extending the observation period to 20 min revealed a plateau in cumulative blood loss, suggesting that bleeding was not only reduced but largely arrested. To further assess efficacy in an external injury context we employed a standardised mouse tail bleeding assay[47]. Following administration of hFA-PT-A1 or control Fc in anti-CD41 antibody-induced thrombocytopenic mice the tail vein was transected, guided on an aluminium bracket to generate a consistent injury depth of approximately 1 mm (Fig. 6e). Thrombocytopenic mice treated with hFA-PT-A1 exhibited a significant reduction in both total blood loss (Fig. 6f) and bleeding duration (Fig. 6g) compared with the Fc control-treated controls indicating that hFA-PT-A1 administration enhances haemostatic responses in vascular trauma under thrombocytopenic conditions.

Finally we evaluated the therapeutic potential of hFA-PT-A1 in a model of spontaneous intestinal haemorrhage. Bleeding was quantified by measuring haemoglobin content in faecal samples (Fig. 6h). To mimic chemotherapy-induced thrombocytopenia we co-administered carboplatin and anti-CD41 antibody. These mice exhibited a marked increase in intestinal bleeding compared with Fc-treated normal controls (Fig. 6i, bar graphs 1 and 2). Importantly injection of hFA-PT-A1 significantly reduced this bleeding (Fig. 6i, bar graphs 2 and 3), despite continued severe platelet depletion (Fig. 6j). These findings indicate that hFA-PT-A1 confers protective haemostatic effects against spontaneous intestinal bleeding in a setting of severe thrombocytopenia, reinforcing its potential as a therapeutic option for managing bleeding complications in thrombocytopenic patients.

Discussion

Recent advances in artificial platelet design have introduced promising strategies for replicating key platelet functions using recombinant or synthetic constructs. Notably several research groups have developed platelet-mimetic particles that can target sites of vascular injury and facilitate localised haemostasis—for example, lipid-based nanoparticles conjugated with von Willebrand factor-binding peptides and fibrinogen-mimetic ligands, which enable platelet recruitment and adhesion at the wound site[48]. Similarly functionalized nanoparticles incorporating Arg-Gly-Asp motifs have demonstrated the ability to enhance fibrin formation and accelerate clot maturation in preclinical bleeding models[49]. However these approaches depend on the presence of functional endogenous platelets to achieve haemostatic efficacy, which limits their applicability in conditions of severe thrombocytopenia.

To address this challenge we developed a recombinant haemostatic proteins composed of chimeric fusion proteins that integrate key endogenous domains responsible for fibrinogen binding, thrombin anchoring and vascular injury targeting. Anchoring thrombin activity at the site of injury appears to be critical for effective haemostasis. Thrombin when activated through the tissue factor-mediated extrinsic pathway and subsequent prothrombinase activity[50], amplifies local coagulation through positive feedback in the coagulation cascade[51]. Consequently localised and sustained thrombin activity facilitates dense fibrin network formation precisely at the injury site, which may be sufficient to halt bleeding even in the absence of functional platelets under controlled conditions (Fig. 1b, c).

Another distinguishing feature of our recombinant haemostatic proteins is its ability to circulate safely in the bloodstream without inducing off-target thrombosis. This is achieved through the intrinsic 'safety lock' mechanism encoded in the N-terminal region of the fibrinogen α-chain[52] which prevents premature fibrin polymerisation in the absence of thrombin activation[53]. By incorporating this thrombin-sensitive domain into the chimeric protein design FA-PT-A1 remains inert under physiological conditions and become selectively activated at sites of vascular injury. This design enables systemic administration without increasing the risk of ectopic clot formation (Fig. 4d).

The dimeric configuration of FA-PT-A1 may further contribute to its haemostatic efficacy by enabling simultaneous interactions with multiple coagulation components particularly fibrin molecules. Each monomer within the dimer contains a fibrinogen α-chain-derived GPR motif and the bivalent nature of the construct allows it to capture two fibrin/fibrinogen molecules simultaneously. This dual engagement likely facilitates cross-linking or local clustering of fibrin strands at the wound site thereby promoting the formation of a denser and more stable fibrin network (Supplementary Fig. 12b). Moreover by increasing avidity toward thrombin, the dimeric FA-PT-A1 construct may enhance polymerisation kinetics. This multivalent interaction model provides a mechanistic explanation for the accelerated fibrin assembly observed in both in vitro and in vivo experiments following FA-PT-A1 administration (Figs. 3g and 5i, j).

The features embedded in these recombinant haemostatic proteins—injury-site specific thrombin anchoring, a built-in safety lock that prevents premature activation, and multivalent interaction that enhances fibrin network formation—appear to confer haemostatic activity while minimising uncontrolled thrombosis. Despite these advantages several limitations remain. Because the strategy lacks platelet-specific functions such as clot retraction and

https://doi.org/10.1038/s41467-026-71344-9

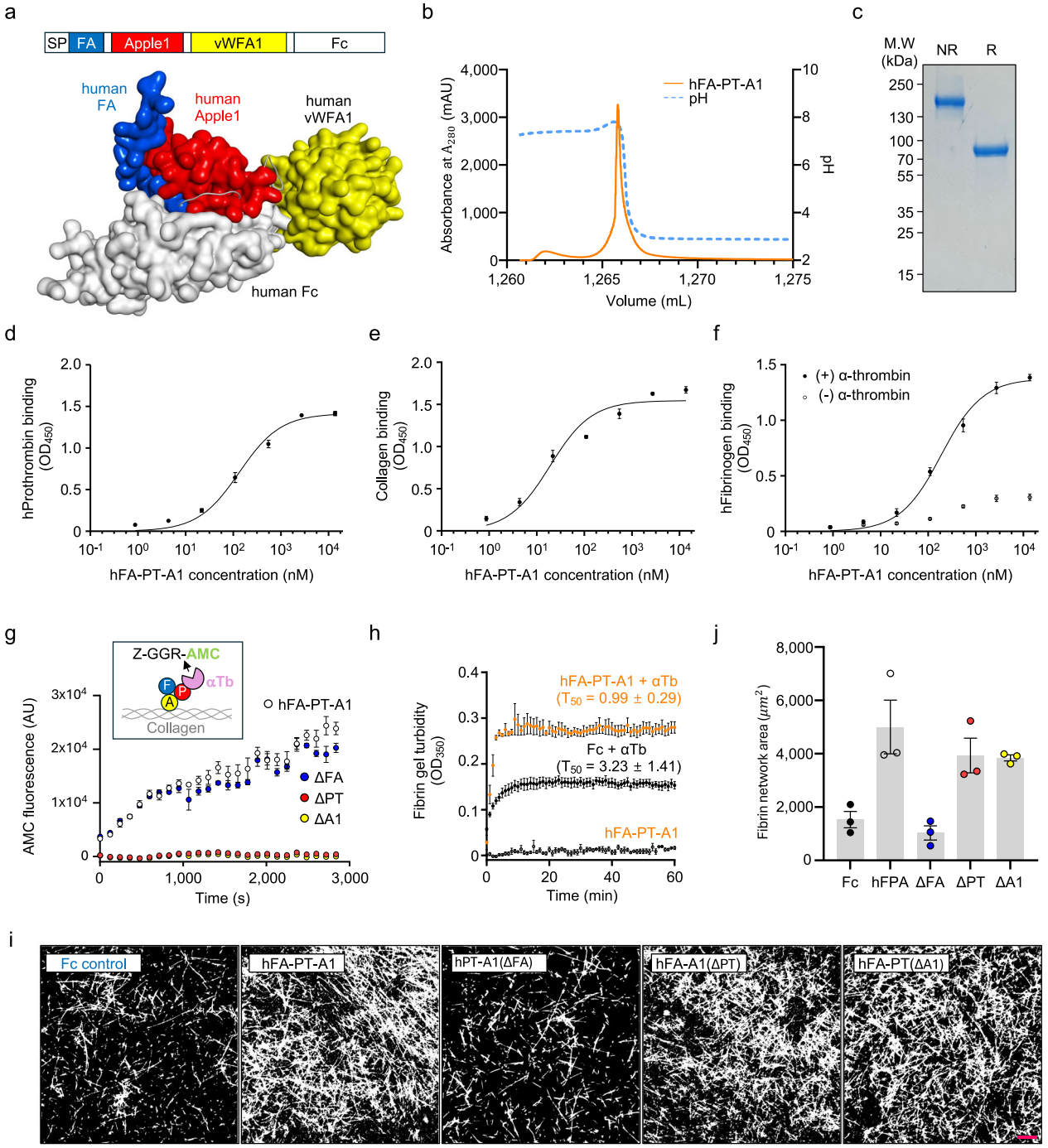

Fig. 5 | Development of hFA-PT-A1 for therapeutic use in human. a AlphaFold-predicted 3D structure of hFA-PT-A1 derived from human proteins. **b** Fc affinity chromatography elution profile. **c** SDS-PAGE analysis under non-reducing (NR) and reducing (R) conditions. Representative data for at least 3 independent experiments are shown. Source data are provided as a Source data file. **d**–**f** Binding of hFA-PT-A1 to human prothrombin bovine collagen and human fibrinogen analysed as in Fig. 1. Experiments were repeated independently at least 3 times with similar results. Error bars represent the mean ± SE ($n = 3$, technical replicates). **g** hFA-PT-A1 or its deletion mutants were applied to collagen-coated surfaces and incubated with α-thrombin. Thrombin activity was measured using the fluorogenic substrate Z-GGR-AMC. Experiments were repeated independently at least 3 times with similar results. Error bars represent the mean ± SE ($n = 3$, technical replicates). **h** Fibrinogen solution was mixed with α-thrombin to initiate fibrin gel formation and turbidity was monitored at an optical density of 350 nm. Experiments were repeated independently at least 3 times with similar results. Error bars represent the mean ± SE ($n = 3$, technical replicates). **i** Fibrin gels were generated by mixing FITC-conjugated and unlabelled fibrinogen (1:9) with Fc control, hFA-PT-A1, or its mutants (20 nM). Confocal images were acquired to a depth of 10 μm at 1 μm intervals and projected into a single image. Representative images are shown. Scale bar, 10 μm. **j** Quantified fibrin densities from (**i**) presented as bar graphs. hFPA, human FA-PT-A1. Error bars represent the mean ± SE ($n = 3$ independent experiments).

https://doi.org/10.1038/s41467-026-71344-9

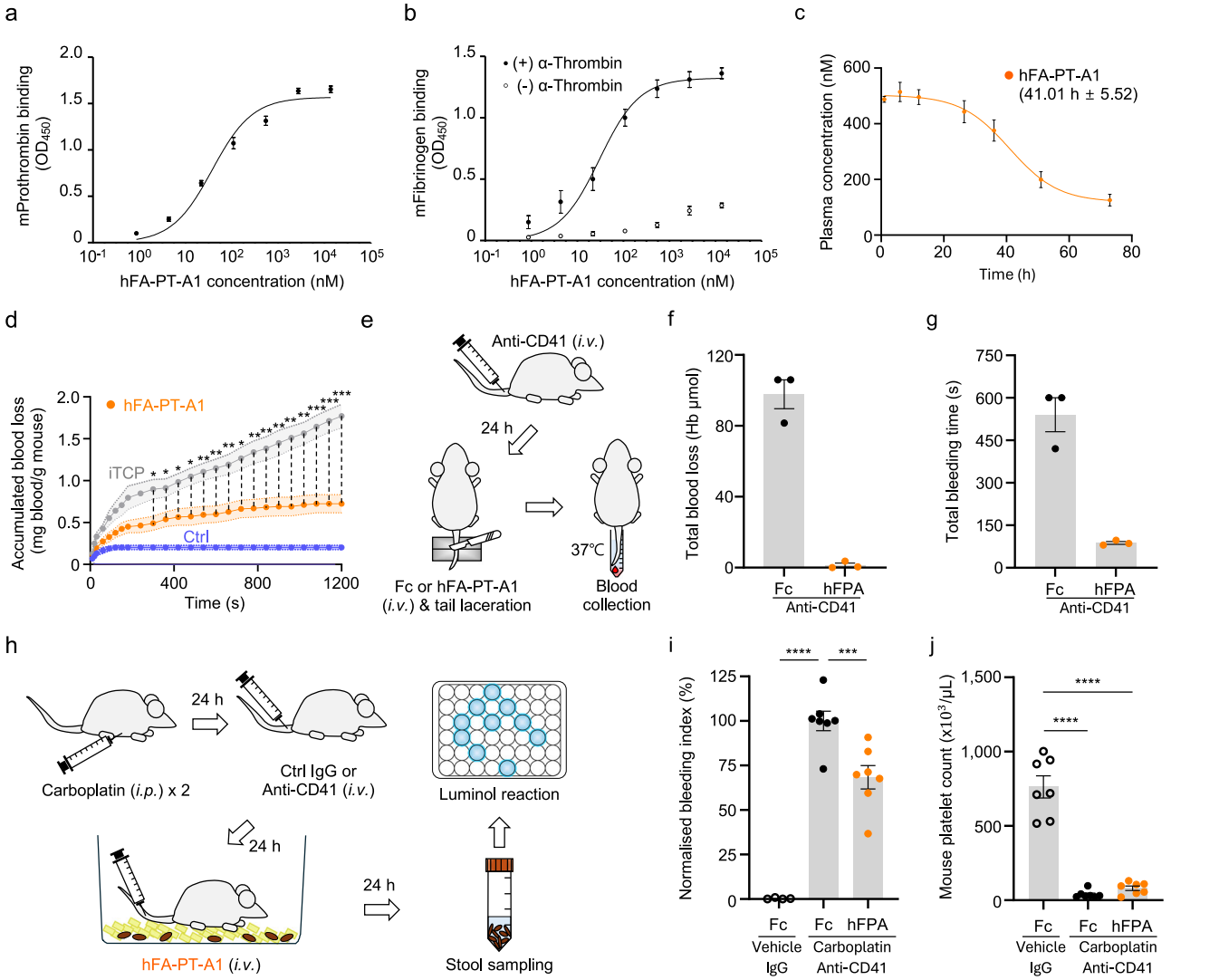

Fig. 6 | Efficacy of hFA-PT-A1 in thrombocytopenic mouse models of trauma and spontaneous bleeding. a, **b** Binding of hFA-PT-A1 to mouse prothrombin and fibrinogen as in Fig. 1. Experiments were repeated independently at least 3 times with similar results. Error bars represent the mean ± SE ($n = 3$, technical replicates). **c** Plasma concentration of hFA-PT-A1 over time as in Fig. 3a. Error bars represent the mean ± SE ($n = 3$ mice per group). **d** Time-dependent accumulated blood loss following liver laceration in the Fc control (Ctrl; blue), anti-CD41-injected (iTCP; grey) and anti-CD41 plus hFA-PT-A1-injected mice (orange). Each graph represents the mean ± SE ($n = 6$ mice per group). Statistical analysis was performed using two-way ANOVA with Dunnett's test. *, $p \le 0.05$ (300 s: 0.0344; 360 s: 0.0436; 420 s: 0.025; 480 s: 0.015; 720 s: 0.0103); **, $p \le 0.01$ (540 s: 0.0092; 600 s: 0.0074; 660 s: 0.0098; 780 s: 0.0062; 840 s: 0.0058; 900 s: 0.0053; 960 s: 0.002; 1020 s: 0.0013); ***, $p \le 0.001$ (1080 s: 0.0007; 1140 s: 0.0004; 1200 s: 0.0003). iTCP, induced-thrombocytopenia. Source data are provided as a Source data file. **e** Schematic diagram of the mouse tail bleeding assay. **f** Total blood loss from lacerated tail quantified via Drabkin's reagent. Error bars represent the mean ± SE ($n = 3$ mice per condition). **g** Total bleeding time in thrombocytopenic mice post-injection with Fc control or hFA-PT-A1. Error bars represent the mean ± SE ($n = 3$ mice per group). Note: 600 s was the observation window. **h** Schematic diagram of chemotherapy-induced thrombocytopenia model. Mice were treated with carboplatin (50 mg/kg) via intraperitoneal (i.p.) injection twice at 24 h intervals, followed by anti-CD41 antibody (0.75 mg/kg) via intravenous injection (i.v.). hFA-PT-A1 or Fc control (5 mg/kg) was administered 24 h later, and faecal samples were collected over the following 24 h. Blood content was measured using luminol assay. **i** Quantitative analysis of residual faecal blood concentration ($n = 7$ mice per group, combined from two independent experiments). To account for inter-experimental variation data were normalised to the mean values from Fc control-treated normal (0%) to thrombocytopenic (100%) and shown as individual dots. One-way ANOVA with Dunnett's test: ***, $p \le 0.001$ (anti-CD41 + carboplatin/Fc vs. anti-CD41 + carboplatin/FPA: 0.0007); ****, $p \le 0.0001$. Source data are provided as a Source data file. **j** Platelet counts under each condition from (**i**). Error bars represent the mean ± SE. One-way ANOVA with Dunnett's test: ****, $p \le 0.0001$. Source data are provided as a Source data file.

amplification mechanisms driven by platelet secretion, their ability to sustain long-term haemostasis is inherently incomplete, as reflected by occasional rebleeding in the tail-laceration assay (Supplementary Fig. 8). Moreover although repeated-dose evaluation did not reveal increased pulmonary microthrombi (Fig. 4d), delayed adverse events cannot be fully excluded and will require continued evaluation in future studies.

Several innovative platelet-mimetic systems have recently been reported each offering valuable insights into how key platelet functions may be reconstructed synthetically. Ultrasoft platelet-like particles for example introduce deformable microgel structures that interact with fibrin networks and partially emulate platelet contractile behaviour[19]. Similarly plasmin-responsive procoagulant nanoparticles provide an elegant strategy for generating a localised phosphatidylserine-rich surface to support thrombin generation[20]. While promising questions remain regarding their anchorage at wound sites, potential dependence on endogenous platelets, and/or the long-term behaviour of those particles under physiological degradation.

Relative to these particle-based systems our recombinant protein-based haemostatic agents have intrinsic advantages. They directly anchor to collagen exposed at vascular injuries and localise thrombin and fibrinogen through defined molecular domains. In addition because their functional domains are encoded at the amino-acid level, they do not require complex post-synthetic surface engineering, rely only on standard antibody-generation platforms for production, and allow reliable batch-to-batch reproducibility.

Taken together our findings indicate that this recombinant protein-based haemostatic agent may offer a viable therapeutic strategy. These constructs could be employed as bridge therapy during platelet transfusion shortages or as an adjunct to reduce the transfusion burden thereby addressing a critical unmet need in the management of bleeding complications in thrombocytopenic patients.

Methods

Animal and ethics statement

Male BALB/c mice (8 weeks old) were used throughout the study for surgical procedures and antibody-induced immune thrombocytopenia. All animal experiments were conducted in compliance with the National Institutes of Health Guide for the Care and Use of Laboratory Animals and all experimental procedures in this study were approved by the Korea University Institutional Animal Care and Use Committee (KUIACUC-2024-0086). Animals were maintained under controlled temperature (23 °C) and humidity conditions (50%) with a 12-h light-dark cycle (light on at 7 AM). Food and water were available ad libitum.

Construction of expression vectors and protein purification

DNA sequence for FA-PT-A1 and hFA-PT-A1 was synthesised and purchased from Integrated DNA Technologies (IDT, IA, USA). For FA-PT-A1 and hFA-PT-A1 each synthesized sequence was PCR-amplified and introduced into pFUSE-hIgG1 (InvivoGen, USA) vector using AgeI and XhoI restriction enzymes. For T17-C6-F7 each selected prothrombin, collagen and fibrinogen-binding scFv clone was PCR-amplified and introduced into the pFUSE-hIgG1 vector using EcoRI, NcoI, EcoRV, XbaI, HindIII and XhoI restriction enzymes. Each scFv was connected by tandem GGGGS linker. When necessary sequences encoding the pre-protrypsin signal peptide, twin-strep tag, or 2B8 tag were inserted. The resulting plasmids were transiently transfected into FreeStyle™ 293-F cell suspension cultures (Thermo Fisher Scientific) using linear poly(ethyleneimine) (MW 25,000, Polysciences). Ten days after transfection the clarified culture media were subjected to fast protein liquid chromatography using an NGC Quest10 Plus system (Bio-Rad) equipped with a 5 mL MabSelectSURE prepacked resin column (Cytiva). Bound proteins were eluted with Pierce™ IgG elution buffer (Thermo Fisher Scientific), neutralised to pH 7.4, mixed with glycerol to a final concentration of 10%, and filtered through Spin-X centrifuge tube filters (Corning, USA). The purified proteins were quantified flash-frozen in liquid nitrogen, and stored at −80 °C for further use.

Phage display library screening

Immunoplate strips (SPL Life Science) were coated with 1 µg of the target protein and blocked with 3% bovine serum albumin (BSA) in Tris-buffered saline (TBS). A phage pool from a single-chain variable fragment library[27] was added to the wells and incubated in the wells for 2 h. After washing with TBS containing 0.5% Tween-20 bound phages were eluted with 100 mM glycine-HCl (pH 2.2), immediately neutralised, and amplified by infecting *E. coli* strain ER2738 in the presence of VSCM13 helper phage overnight. The amplified phages were precipitated using polyethylene glycol and resuspended in TBS containing 1% BSA, and used as the input pool for subsequent rounds. To calculate the output/input ratio both the initial phage pool and eluted phages were titrated by counting the colony-forming units. For phage binding assays periplasmic fractions were prepared[27] and applied to Immunoplate strips coated with the target protein. Bound scFvs tagged with an N-terminal HA tag, were detected using an anti-HA antibody conjugated with horseradish peroxidase (HRP), followed by reaction with tetramethylbenzidine substrate (Thermo Fisher Scientific).

Mouse liver laceration model

Male BALB/c mice (8 weeks old) were intravenously injected with anti-CD41 antibody (MWReg30, Biolegend; 0.75 mg/kg) to induce thrombocytopenia. After 24 h FA-PT-A1, T17-C6-F7 or hFA-PT-A1 was administered intravenously at a dose of 5 mg/kg. Thirty minutes later mice were anaesthetised with a constant flow of isoflurane. A 3-mm horizontal cut was made on the left liver lobe using a surgical blade (#20). Immediately after laceration a pre-weighed sterile cotton gauze was placed on the wound to absorb blood. At 10, 20, 30, 60, 90, 120, 150, 180, 210, 240, 300, 360, 420, 480, 540 and 600 s, the gauze was removed and reweighed to quantify blood loss. For hFA-PT-A1 experiment at 10, 20, 30, 60, 90, 120, 150, 180, 210, 240, 300, 360, 420, 480, 540, 600, 660, 720, 780, 840, 900, 960, 1020, 1080, 1140 and 1200 s, the gauze was removed and reweighed to quantify blood loss. For topical treatment FA-PT-A1 or T17-C6-F7 was mixed with 1% (w/v) sodium alginate (Sigma-Aldrich) at a final concentration of 500 nM. Immediately after laceration 100 µL of the premixed haemostatic hydrogel was applied directly to the wound site. To initiate gelation 4 µL of 50 mM $CaCl_2$ was added and mixed with the hydrogel. The liver laceration procedure was video-recorded and time-lapse images were extracted at 30-s intervals. Bleeding time was defined as the time point at which image subtraction from preceding frames showed no detectable difference. Platelet counts were measured using a haematology analyser (BC-2800 Vet, Mindray).

Mouse pulmonary microthrombi formation assay

Male mice were intravenously injected with saline mucin (0.5 mg/kg), FA-PT-A1 (5 mg/kg) or T17-C6-F7 (5 mg/kg). After euthanasia lungs were surgically harvested and fixed with 4% paraformaldehyde. Lungs were inflated by injecting 50% O.C.T compound (Tissue-Tek) in phosphate-buffered saline (PBS) dehydrated in 30% sucrose, embedded in O.C.T compound, and stored at −80 °C. Cryosectioning was performed using a cryostat (CM-1850, Leica) at a thickness of 10 µm. Tissue sections were stained with goat anti-human IgG Fc (1:100; Invitrogen) and mouse anti-fibrinogen α-chain antibody (UC45, 1:100).

Mouse tail-vein laceration assay

Tails of anti CD41-induced thrombocytopenic mice were pre-soaked in a 37 °C water bath for 5 min placed on a tail laceration guidance bracket[44], and cut at the vein using a surgical knife (blade #20) guided by the bracket's horizontal groove. Wounded tails were immersed in pre-warmed saline to collect shed blood. Red blood cells were pelleted by centrifugation and lysed in 1 mL of Drabkin's reagent (Sigma-Aldrich, USA). Each sample was diluted to 1:250 in Drabkin's reagent incubated for 15 min, and analysed using a spectrometer. Total blood loss was calculated in haemoglobin (Hb) nmol units based on a standard curve generated using purified haemoglobin (Merck).

Mouse spontaneous intestinal bleeding model

Mice were intraperitoneally injected with carboplatin (Sigma-Aldrich) at a dose of 50 mg/kg administered twice at 24-h intervals, followed by intravenous injection of anti-CD41 antibody. Mice were then treated with hFA-PT-A1 (5 mg/kg) and housed in separate cages for 24 h. Faecal samples were collected and lysed by incubation in 20 mL of 0.53 M potassium hydroxide at 37 °C for 1 h. The lysates were centrifuged at 17,000 × *g* at 4 °C, and 5 µL of the supernatant was mixed with 95 µL of luminol solution (0.53 M KOH, 1.5% H_2O_2, 0.04% luminol). Chemiluminescence was measured immediately at 415 nm using a microplate reader (SpectraMax i3x, San Jose, CA, USA).

Surface plasmon resonance

SPR was performed on a Biacore T200 at 25 °C. Ligands were immobilised on a CM5 chip via amine coupling: the surface was activated with 1:1 0.4 M EDC/0.1 M NHS, followed by ligand injection (5 μL/min) in 10 mM sodium acetate (pH 4.5–5.5) to target RU, and blocked with 1 M ethanolamine-HCl (pH 8.5). A reference cell was prepared identically without the ligand. Binding assays utilised HBS-EP+ running buffer (10 mM HEPES, 150 mM NaCl, 3 mM EDTA, 0.05% P20, pH 7.4). Series of diluted analytes were injected at 30 μL/min for a 180 s association and 180 s dissociation phase. The surface was regenerated after each cycle using 10 mM glycine-HCl (pH 2.5) or 5 M NaCl for 30 s at 30 μL/min, followed by a 60 s stabilisation period. Sensorgrams were processed with Biacore T200 evaluation software using reference cell subtraction. Kinetic data were globally fitted to a 1:1 Langmuir model to determine k_a, k_d, and K_D; steady-state affinity was calculated by plotting R_{eq} against concentration for experiments reaching equilibrium.

Statistical analysis

All data are presented as mean ± standard error of the mean (SEM), unless otherwise noted. One-way and two-way analyses of variance (ANOVA), followed by Dunnett's method for multiple comparisons, were used to compare experimental groups unless otherwise specified. A p-value less than 0.05 was considered statistically significant. Statistical analyses were performed using GraphPad Prism version 10 (La Jolla, CA, USA).

Reporting summary

Further information on research design is available in the Nature Portfolio Reporting Summary linked to this article.

Data availability

All data are available in the main text or in the Supplementary Information. Source data are provided with this paper. For original data and other information, please contact chungho@korea.ac.kr Source data are provided with this paper.

References

1. Rumbaut, R. E. & Thiagarajan, P. *Platelet-Vessel Wall Interactions in Hemostasis and Thrombosis* (Morgan & Claypool Life Sciences, 2010).
2. Ho-Tin-Noe, B. & Jadoui, S. Spontaneous bleeding in thrombocytopenia: is it really spontaneous? *Transfus. Clin. Biol.* **25**, 210–216 (2018).
3. Yougbare, I. et al. Maternal anti-platelet beta3 integrins impair angiogenesis and cause intracranial hemorrhage. *J. Clin. Investig.* **125**, 1545–1556 (2015).
4. Psaila, B. et al. Intracranial hemorrhage (ICH) in children with immune thrombocytopenia (ITP): study of 40 cases. *Blood* **114**, 4777–4783 (2009).
5. Semple, J. W., Italiano, J. E. Jr. & Freedman, J. Platelets and the immune continuum. *Nat. Rev. Immunol.* **11**, 264–274 (2011).
6. Wang, L. et al. First line treatment of adult patients with primary immune thrombocytopenia: a real-world study. *Platelets* **31**, 55–61 (2020).
7. Hsia, C. C. et al. Intravenous immunoglobulin (IVIg) utilization in immune thrombocytopenia (ITP): a multi-center, retrospective review. *Drugs Real World Outcomes* **2**, 35–42 (2015).
8. Lucchini, E., Zaja, F. & Bussel, J. Rituximab in the treatment of immune thrombocytopenia: what is the role of this agent in 2019? *Haematologica* **104**, 1124–1135 (2019).
9. Gonzalez-Lopez, T. J. & Provan, D. The new era of primary immune thrombocytopenia management in adults: a narrative review of current and emerging treatments. *Blood Rev.* **73**, 101300 (2025).
10. Chaturvedi, S., Arnold, D. M. & McCrae, K. R. Splenectomy for immune thrombocytopenia: down but not out. *Blood* **131**, 1172–1182 (2018).
11. Neunert, C. et al. American Society of Hematology 2019 guidelines for immune thrombocytopenia. *Blood Adv.* **3**, 3829–3866 (2019).
12. Kuter, D. J. Managing thrombocytopenia associated with cancer chemotherapy. *Oncology* **29**, 282–294 (2015).
13. Shaw, J. L., Nielson, C. M., Park, J. K., Marongiu, A. & Soff, G. A. The incidence of thrombocytopenia in adult patients receiving chemotherapy for solid tumors or hematologic malignancies. *Eur. J. Haematol.* **106**, 662–672 (2021).
14. Kuter, D. J. Treatment of chemotherapy-induced thrombocytopenia in patients with non-hematologic malignancies. *Haematologica* **107**, 1243–1263 (2022).
15. Song, A. B. & Al-Samkari, H. Chemotherapy-induced thrombocytopenia: modern diagnosis and treatment. *Br. J. Haematol.* **206**, 1062–1066 (2025).
16. Kaufman, R. M. et al. Platelet transfusion: a clinical practice guideline from the AABB. *Ann. Intern. Med.* **162**, 205–213 (2015).
17. Srivastava, A. et al. WFH guidelines for the management of hemophilia, 3rd edition. *Haemophilia* **26**, 1–158 (2020).
18. Anselmo, A. C. et al. Platelet-like nanoparticles: mimicking shape, flexibility, and surface biology of platelets to target vascular injuries. *ACS Nano* **8**, 11243–11253 (2014).
19. Nellenbach, K. et al. Ultrasoft platelet-like particles stop bleeding in rodent and porcine models of trauma. *Sci. Transl. Med.* **16**, eadi4490 (2024).
20. Sekhon, U. D. S. et al. Platelet-mimicking procoagulant nanoparticles augment hemostasis in animal models of bleeding. *Sci. Transl. Med.* **14**, eabb8975 (2022).
21. Mackman, N., Tilley, R. E. & Key, N. S. Role of the extrinsic pathway of blood coagulation in hemostasis and thrombosis. *Arterioscler. Thromb. Vasc. Biol.* **27**, 1687–1693 (2007).
22. Pieters, M. et al. An international study on the standardization of fibrin clot permeability measurement: methodological considerations and implications for healthy control values. *J. Thromb. Haemost.* **10**, 2179–2181 (2012).
23. Blomback, B. et al. Native fibrin gel networks observed by 3D microscopy, permeation and turbidity. *Biochim. Biophys. Acta* **997**, 96–110 (1989).
24. Weisel, J. W. & Litvinov, R. I. Mechanisms of fibrin polymerization and clinical implications. *Blood* **121**, 1712–1719 (2013).
25. Coppens, M., Eikelboom, J. W., Gustafsson, D., Weitz, J. I. & Hirsh, J. Translational success stories: development of direct thrombin inhibitors. *Circ. Res.* **111**, 920–929 (2012).
26. Baglia, F. A., Badellino, K. O., Ho, D. H., Dasari, V. R. & Walsh, P. N. A binding site for the Kringle II domain of prothrombin in the Apple 1 domain of factor XI. *J. Biol. Chem.* **275**, 31954–31962 (2000).
27. Flood, V. H. et al. Crucial role for the VWF A1 domain in binding to type IV collagen. *Blood* **125**, 2297–2304 (2015).
28. Jumper, J. et al. Highly accurate protein structure prediction with AlphaFold. *Nature* **596**, 583–589 (2021).
29. Yang, H. Y., Kang, K. J., Chung, J. E. & Shim, H. Construction of a large synthetic human scFv library with six diversified CDRs and high functional diversity. *Mol. Cells* **27**, 225–235 (2009).
30. Smith, G. P. Filamentous fusion phage: novel expression vectors that display cloned antigens on the virion surface. *Science* **228**, 1315–1317 (1985).
31. van Rosmalen, M., Krom, M. & Merkx, M. Tuning the flexibility of glycine-serine linkers to allow rational design of multidomain proteins. *Biochemistry* **56**, 6565–6574 (2017).
32. Schmidt, T. G. & Skerra, A. The Strep-tag system for one-step purification and high-affinity detection or capturing of proteins. *Nat. Protoc.* **2**, 1528–1535 (2007).

33. Kim, T. L., Cho, M. H., Sangsawang, K. & Bhoo, S. H. Fine mutational analysis of 2B8 and 3H7 tag epitopes with corresponding specific monoclonal antibodies. *Mol. Cells* **39**, 460–467 (2016).
34. Mangeat, T. et al. Fc-engineered monoclonal antibodies to reduce off-target liver uptake. *EJNMMI Res.* **13**, 81 (2023).
35. Deng, R. & Balthasar, J. P. Comparison of the effects of antibody-coated liposomes, IVIG, and anti-RBC immunotherapy in a murine model of passive chronic immune thrombocytopenia. *Blood* **109**, 2470–2476 (2007).
36. Morowski, M. et al. Only severe thrombocytopenia results in bleeding and defective thrombus formation in mice. *Blood* **121**, 4938–4947 (2013).
37. Sheridan, A. et al. Clot-targeted nanogels for dual-delivery of antithrombinIII and tissue plasminogen activator to mitigate disseminated intravascular coagulation complications. *ACS Nano* **18**, 15517–15528 (2024).
38. Ackermann, M. et al. Pulmonary vascular endothelialitis, thrombosis, and angiogenesis in Covid-19. *New Engl. J. Med.* **383**, 120–128 (2020).
39. Wahrenbrock, M., Borsig, L., Le, D., Varki, N. & Varki, A. Selectin-mucin interactions as a probable molecular explanation for the association of Trousseau syndrome with mucinous adenocarcinomas. *J. Clin. Investig.* **112**, 853–862 (2003).
40. Ueki, H. et al. Neutrophil adhesion to vessel walls impairs pulmonary circulation in COVID-19 pathology. *Nat. Commun.* **16**, 455 (2025).
41. Fidler, A. L., Boudko, S. P., Rokas, A. & Hudson, B. G. The triple helix of collagens—an ancient protein structure that enabled animal multicellularity and tissue evolution. *J. Cell Sci.* **131**, jcs20395 (2018).
42. Spraggon, G., Everse, S. J. & Doolittle, R. F. Crystal structures of fragment D from human fibrinogen and its crosslinked counterpart from fibrin. *Nature* **389**, 455–462 (1997).
43. Kononova, O. et al. Molecular mechanisms, thermodynamics, and dissociation kinetics of knob-hole interactions in fibrin. *J. Biol. Chem.* **288**, 22681–22692 (2013).
44. Fowler, W. E., Hantgan, R. R., Hermans, J. & Erickson, H. P. Structure of the fibrin protofibril. *Proc. Natl. Acad. Sci. USA* **78**, 4872–4876 (1981).
45. Mosesson, M. W., DiOrio, J. P., Siebenlist, K. R., Wall, J. S. & Hainfeld, J. F. Evidence for a second type of fibril branch point in fibrin polymer networks, the trimolecular junction. *Blood* **82**, 1517–1521 (1993).
46. Carr, M. E. Jr. & Hermans, J. Size and density of fibrin fibers from turbidity. *Macromolecules* **11**, 46–50 (1978).
47. Johansen, P. B., Tranholm, M., Haaning, J. & Knudsen, T. Development of a tail vein transection bleeding model in fully anaesthetized haemophilia A mice-characterization of two novel FVIII molecules. *Haemophilia* **22**, 625–631 (2016).
48. Haji-Valizadeh, H., Modery-Pawlowski, C. L. & Sen Gupta, A. A factor VIII-derived peptide enables von Willebrand factor (VWF)-binding of artificial platelet nanoconstructs without interfering with VWF-adhesion of natural platelets. *Nanoscale* **6**, 4765–4773 (2014).
49. Bertram, J. P. et al. Intravenous hemostat: nanotechnology to halt bleeding. *Sci. Transl. Med* **1**, 11ra22 (2009).
50. Hoffman, M. Remodeling the blood coagulation cascade. *J. Thromb. Thrombolysis* **16**, 17–20 (2003).
51. Rosing, J., Tans, G., Govers-Riemslag, J. W., Zwaal, R. F. & Hemker, H. C. The role of phospholipids and factor Va in the prothrombinase complex. *J. Biol. Chem.* **255**, 274–283 (1980).
52. Nossel, H. L. et al. Measurement of fibrinopeptide A in human blood. *J. Clin. Investig.* **54**, 43–53 (1974).
53. Brummel, K. E., Paradis, S. G., Butenas, S. & Mann, K. G. Thrombin functions during tissue factor-induced blood coagulation. *Blood* **100**, 148–152 (2002).

Acknowledgements

This work was supported by the Basic Science Research Program through the National Research Foundation of Korea (grant numbers 2022M3E5F2018367 and RS-2025-00520706) and a Korea University Grant. We thank Dr. Myung Hee Nam for assistance with SPR analysis at KBSI.

Author contributions

C.G.L., S.J.H. and C.K. designed the study. C.G.L., J.L., G.S. and J.M.K. performed the experiments. C.G.L., J.L., G.S., J.M.K., H.S., J.Y.P., H.W.C. and C.K. analysed the data. C.G.L. wrote the manuscript, which was edited by C.K., S.J.H. and J.Y.P.

Competing interests

C.G.L., J.L. and C.K. intend to file a patent application based on the findings reported in this manuscript. The remaining authors declare no competing interests.

Additional information

Supplementary information The online version contains Supplementary material available at https://doi.org/10.1038/s41467-026-71344-9.

Correspondence and requests for materials should be addressed to Chungho Kim.

Peer review information *Nature Communications* thanks Ching-Ping Tseng and the other anonymous reviewer(s) for their contribution to the peer review of this work. A peer review file is available.

Reprints and permissions information is available at http://www.nature.com/reprints

Publisher's note Springer Nature remains neutral with regard to jurisdictional claims in published maps and institutional affiliations.

Open Access This article is licensed under a Creative Commons Attribution-NonCommercial-NoDerivatives 4.0 International License, which permits any non-commercial use, sharing, distribution and reproduction in any medium or format, as long as you give appropriate credit to the original author(s) and the source, provide a link to the Creative Commons licence, and indicate if you modified the licensed material. You do not have permission under this licence to share adapted material derived from this article or parts of it. The images or other third party material in this article are included in the article's Creative Commons licence, unless indicated otherwise in a credit line to the material. If material is not included in the article's Creative Commons licence and your intended use is not permitted by statutory regulation or exceeds the permitted use, you will need to obtain permission directly from the copyright holder. To view a copy of this licence, visit http://creativecommons.org/licenses/by-nc-nd/4.0/.

© The Author(s) 2026